



# Defluoridation using novel chemically treated carbonized bone meal: batch and dynamic performance with scale-up studies

Somak Chatterjee<sup>1</sup> · Munmun Mukherjee<sup>1</sup> · Sirshendu De<sup>1</sup>

Received: 14 December 2017 / Accepted: 12 April 2018 / Published online: 25 April 2018  
© Springer-Verlag GmbH Germany, part of Springer Nature 2018

## Abstract

Novel defluoridating adsorbent was synthesized by chemical treatment of carbonized bone meal using aluminum sulfate and calcium oxide. Precursor for chemical treatment was prepared by partial carbonization of raw bone meal at 550 °C for 4 h. Maximum fluoride removal capacity was 150 mg/g when carbonized bone meal (100 g/L) was treated with aluminum sulfate (500 g/L) and calcium oxide (15 g/L). Morphological analysis revealed formation of a coating layer consisting of aluminum compounds on the precursor surface. This was verified by stretching frequency of aluminum hydroxide (602 cm<sup>-1</sup>) in the infrared spectra. Presence of hydroxylapatite ( $2\theta = 30^\circ$  and  $2\theta = 24^\circ$ ) and aluminum mineral phases ( $2\theta = 44^\circ$ ) in the adsorbent were identified from the X-ray diffractograms. Adsorption capacity decreased from 150 mg/g (30 °C) to 120 mg/g (50 °C) indicating exothermic adsorption. Adsorption experiments under batch kinetic mode were simulated using shrinking core model. Effective fluoride diffusivity in the adsorbent and the mass transfer coefficient were estimated as  $5.8 \times 10^{-12}$  m<sup>2</sup>/s and  $9 \times 10^{-4}$  m/s, respectively. Desorption was maximum at basic pH and desorption efficiency was decreased by 31% after third cycle. Dynamic filtration with artificially fluoride-spiked solution showed that the empty bed contact time for a packed column with equal weight of carbonized and chemically treated adsorbent was 4.7 min and number of bed volumes treated (till WHO limit of 1.5 mg/L) was 340 for a column of 3-cm diameter and 18-cm length. The system was successfully tested using contaminated groundwater from an affected area. Fixed-bed column experiments were simulated from the first principles using convective pore diffusion-adsorption model for both synthetic solution and contaminated groundwater. Axial dispersion coefficient was found to be one order of magnitude less than the pore diffusivity indicating dominance of fluoride diffusion within porous network of adsorbent. The developed adsorbent exhibited antibacterial property as well.

**Keywords** Chemical treatment · Carbonized bone meal · Fluoride · Adsorption · Fixed bed · Scale up

## Introduction

Contamination of groundwater by organic and inorganic pollutants poses serious threat to human health. Organic pollutants, such as pesticides, phenyls, and dioxins, are biodegradable and are consumed by specific bacteria, in their metabolic cycle. For example, a common insecticide, dichloro-diphenyl-

trichloroethane (DDT), is biologically degraded by *Aspergillus flavus* and *Aspergillus parasiticus* species (Katole et al. 2013). However, inorganic pollutants, being non-biodegradable, are persistent in groundwater. Some of the hazardous inorganic pollutants, like arsenic, fluoride, and nitrate, are detrimental for human health (Moore 2012). Among these, fluoride is the 13th abundant element and is an important micronutrient to the human body. But its overdose can cause serious health problems, like nerve paralysis, deformation of skin tissues, and skeletal and dental cavities (fluorosis) (Ozsvath 2009). Fluoride contamination in groundwater occurs due to geochemical weathering of rocks, such as fluorapatite, industrial discharges from aluminum smelters, and copper and zinc ore processing sectors (Ozsvath 2009). World health Organization (WHO) strictly recommends the maximum allowable limit of fluoride concentration in drinking water as 1.5 mg/L (World Health Organization 2004).

Responsible editor: Guilherme L. Dotto

**Electronic supplementary material** The online version of this article (<https://doi.org/10.1007/s11356-018-2025-z>) contains supplementary material, which is available to authorized users.

✉ Sirshendu De  
sde@che.iitkgp.emet.in

<sup>1</sup> Department of Chemical Engineering, Indian Institute of Technology Kharagpur, Kharagpur, India

Fluoride is generally present in areas having semi-arid climate, abundant with crystal and volcanic bed rocks (Brindha and Elango 2011). Such conditions prevail in countries, like Brazil, Chile, Argentina, and northeastern parts of Africa, Pakistan, China, and India (Brindha and Elango 2011). In India, fluoride is excessive in calcium-deficit groundwater, mainly in states of Rajasthan, Madhya Pradesh, Andhra Pradesh, and West Bengal (Brindha and Elango 2011). Fluoride forms coordinate complexes, such as  $\text{HF}^{2-}$  and  $\text{HF}^0$  with water (Mohapatra et al. 2009), and concentration of these complexes is pH dependent. These complexes are bound easily to electropositive elements, like aluminum, calcium, iron, and magnesium (Mohapatra et al. 2009). This principle has been the basis of several treatment methodologies, like adsorption, precipitation, coagulation, and even pressure-driven membrane processes (Tor et al. 2009; Guo and Tian 2013; Gong et al. 2012; Ndiaye et al. 2005). However, adsorption is a comparatively useful process than others, owing to its simplicity in design, ease of operation, and reusability of adsorbent (Faust and Aly 2013). Therefore, adsorbents with high aluminum and calcium content are ideal for fluoride uptake from drinking water. Activated alumina and calcite are the most common ones (Ghorai and Pant 2005; Turner et al. 2010). Possibility of using iron ores, like hematite and magnetite, has also been explored (Sujana et al. 2009). However, most of these adsorbents have low fluoride uptake capacity and require frequent regeneration. To overcome these limitations, researchers have carried extensive works regarding the usage of carbon-based calcium adsorbents (Sivasankar et al. 2012). For example, mammalian bones are rich in calcium and they can be charred either in presence or in absence of air to realign the apatite structure to enhance fluoride uptake capacity (Tchomgui-Kamga et al. 2010a, b). Process of charring (pyrolysis or partial carbonization), calcium-to-phosphate ratio of raw material, charring time, and temperature are some influencing factors in fluoride adsorption (Tchomgui-Kamga et al. 2010a, b). Pyrolysis is conducted at high temperature in presence of inert gas (like argon and nitrogen). Compared to this, partial carbonization requires lower operating temperature in absence of any external gas. Therefore, partial carbonization is less energy intensive and economic compared to pyrolysis. However, adsorbents synthesized by partial carbonization have comparable defluoridation capacity with the ones made from pyrolysis (Rojas-Mayorga et al. 2013; Czernik 2008). After charring of these adsorbents, their defluoridation capacity can be improved further by impregnation of functional chemical groups. For example, defluoridation capacity was increased from 4 to 19 mg/g by impregnation of calcium group in charcoal prepared at 650 °C (Tchomgui-Kamga et al. 2010a, b). When this charcoal was treated with aluminum and iron, fluoride sorption capacity increased to 13 mg/g (Tchomgui-Kamga et al., 2010a, b). Fluoride uptake capacity was doubled due to chemical impregnation of aluminum and

iron on corrosion products (García-Sánchez et al. 2013). However, precursor of these sorbents, i.e., Scandinavian spruce wood or corrosion products, is scarcely distributed and hence it is difficult to produce them in bulk scale for subsequent use in large-scale filters. Additionally, these adsorbents result high-pressure drop in the bed due to low particle size, thereby creating operational difficulties (Dikinya et al. 2008). Therefore, it is essential to synthesize an adsorbent from a naturally available and cost-effective raw material which has high fluoride uptake capacity and breakthrough life in a packed bed with adequate particle size. Raw bone meal (RBM), a mixture of bones like chicken and cattle, is an abundant waste product and is utilized by fertilizer-producing companies (Gao et al. 2009).

This study deals with optimization of scalable synthesis route of chemically treated carbonized adsorbent, made from bone meal including its detailed characterization, followed by application in fluoride removal from groundwater. Effect of different operating conditions in fluoride uptake capacity of the material under batch and fixed-bed study has been performed. Mechanism of adsorption including maximum adsorption capacity was evaluated by fitting the equilibrium data of fluoride uptake with different empirical and statistical isotherm models. Adsorption kinetics was simulated using shrinking core model to obtain more insight of time-varying behavior of adsorption. Fixed-bed column runs were also conducted including variation of operating conditions (bed height, flow rate, and inlet fluoride concentration) to observe the fluoride removal capacity. These experiments were simulated from the first principles using pore diffusion-adsorption model. Different physical parameters characterizing transport properties of fixed bed were also evaluated and used for scaling up calculations. Performance curves of scaled-up filter for different operating and geometrical conditions were also established. Efficacy of the proposed adsorbent in treatment of real-life contaminated groundwater was also investigated in fixed-bed columns.

## Experimental methods

### Materials

RBM, industrial grade hydrochloric acid, and sodium hydroxide (industrial grade reagents) were supplied by M/s, Anupam Enterprise, Kharagpur, West Bengal, India (GPS location: 22.32° N, 87.32° E). Sodium fluoride (molecular weight, 42 g/mol), obtained from M/s, Merck Ltd., Mumbai, India, was dissolved in distilled water to prepare stock solution of fluoride (1000 mg/L). Chemicals, like aluminum sulfate, calcium oxide, sodium chloride, sodium nitrate, sodium carbonate, and ammonium phosphate, were all of analytical grades and obtained from the same company.

## Preparation of chemically treated carbonized bone meal

Initially, RBM was washed properly in hot water (60 °C) for 2 h to remove any impurities and dried thereafter. Samples within size range of 1–2 mm were sieved and placed in silica crucibles, covered with lids. They were then partially carbonized by placing the crucibles in muffle furnace (manufactured by Asian Test Equipments, Uttar Pradesh, India) of internal volume 42.5 l, requiring power source of 220-V and 50-Hz single phase. The samples were prepared at various temperature and duration at constant heating rate 60 °C/min, without gas supply. Optimum carbonization conditions were identified resulting in adsorbent having the highest defluoridation capacity. Carbonized bone meal (CBM) samples prepared at these conditions were subjected to further chemical treatment. One hundred grams of CBM was stirred in 1 l of water, containing calcium oxide for 2 h, followed by addition of aluminum sulfate, and the mixture was stirred for 4 h. After chemical treatment, the final product was filtered, dried, and grinded. Effect of the carbonization and chemical treatment conditions on fluoride adsorption capacity is presented in Table S1 (a) and (b). Preparation method of chemically treated carbonized bone meal (CTBM) and its application in contaminated water treatment is shown in Fig. 1.

## Adsorbent characterization

Morphology analysis of CBM and CTBM was conducted by using FESEM (field emission scanning electron microscope, model: JSM-7610, JEOL, Japan). Mineralogical phases of the prepared adsorbents were identified using X-ray diffractometer (model: Xpert Pro, M/s, PANalytical, The Netherlands). Weight loss of adsorbent with temperature was observed using thermogravimetric analyzer (TGA) (model: Pyris Diamond, Perkin Elmer, Connecticut, USA). Functional groups of the prepared adsorbents were recognized by Fourier transform infrared spectrophotometer (FTIR, model: Spectrum 100, Perkin Elmer, Connecticut, USA). Surface area was measured using Brunner-Emmett-Teller (BET) surface area analyzer (model AUTOSORB-1, Quantachrome Instruments, Florida, USA). Fluoride concentration in different samples was measured by ion selective electrode (model: Orion 720A+, Thermo Electron Corporation, Beverly, USA). Interference effect in fluoride determination by electrode was prevented by dissolving TISAB III in the filtrate (0.1 times the sample volume). Concentration of other coexisting anions, like sulfate, nitrate, carbonate, phosphate, and chloride, was measured by ion chromatograph (model: 883 Basic IC Plus, Metrohm, Switzerland). Concentration of cations, i.e., calcium and aluminum, was measured using atomic absorption spectrophotometer

(model: Aanalyst 700 coupled with MHS-15, Perkin Elmer, Connecticut, USA). Average of five measured concentrations was reported.

## Batch adsorption experiments

Batch study (Chatterjee and De 2016) was conducted in two parts, i.e., equilibrium and kinetics. They are described in the following sections.

### Equilibrium studies

#### Effect of dose, size, and pH

Equilibrium studies were carried out to observe the effect of adsorbent size, concentration, and pH on removal efficiency. Effect of adsorbent size and concentration was carried at 10 mg/L fluoride concentration in feed at 30 °C, 150-rpm shaker speed, and neutral pH (Chatterjee and De 2016). Solution pH was adjusted with base or acid to study the effect of pH.

#### Effect of temperature

In order to obtain maximum uptake capacity and analyze the effect of temperature on adsorption, different solutions having feed concentration in the range of 20 to 1000 mg/L were equilibrated in a shaker at 30, 40, and 50 °C (adsorbent concentration 7 g/L; stirrer speed of 150 rpm). Amount of fluoride adsorbed by CTBM was evaluated using the mass balance (Chatterjee and De 2016),

$$q_e = \frac{(C_o - C_e)v}{m} \quad (1)$$

where,  $q_e$  (mg/g) is the amount of fluoride adsorbed by CTBM,  $C_o$  and  $C_e$  are the initial and equilibrium concentration (mg/L),  $v$  is the volume of the solution (L), and  $m$  is the amount of adsorbent used (g). The data sets obtained at different temperatures were fitted to three empirical isotherm models, i.e., Langmuir, Freundlich, and Dubinin-Radushkevich (D-R) (Foo and Hameed 2010). However, in order to describe the interaction between CTBM and fluoride ions precisely, Hill's model, directly derived from statistical physics, was used as well (Sellaoui et al. 2017a, b; Sellaoui et al. 2016). Discussion related to the utility of the isotherm models and their characteristic equations is presented in Supplementary Section S1. Theory behind thermodynamic calculations for adsorption of fluoride by CTBM is given in Supplementary Section S2.

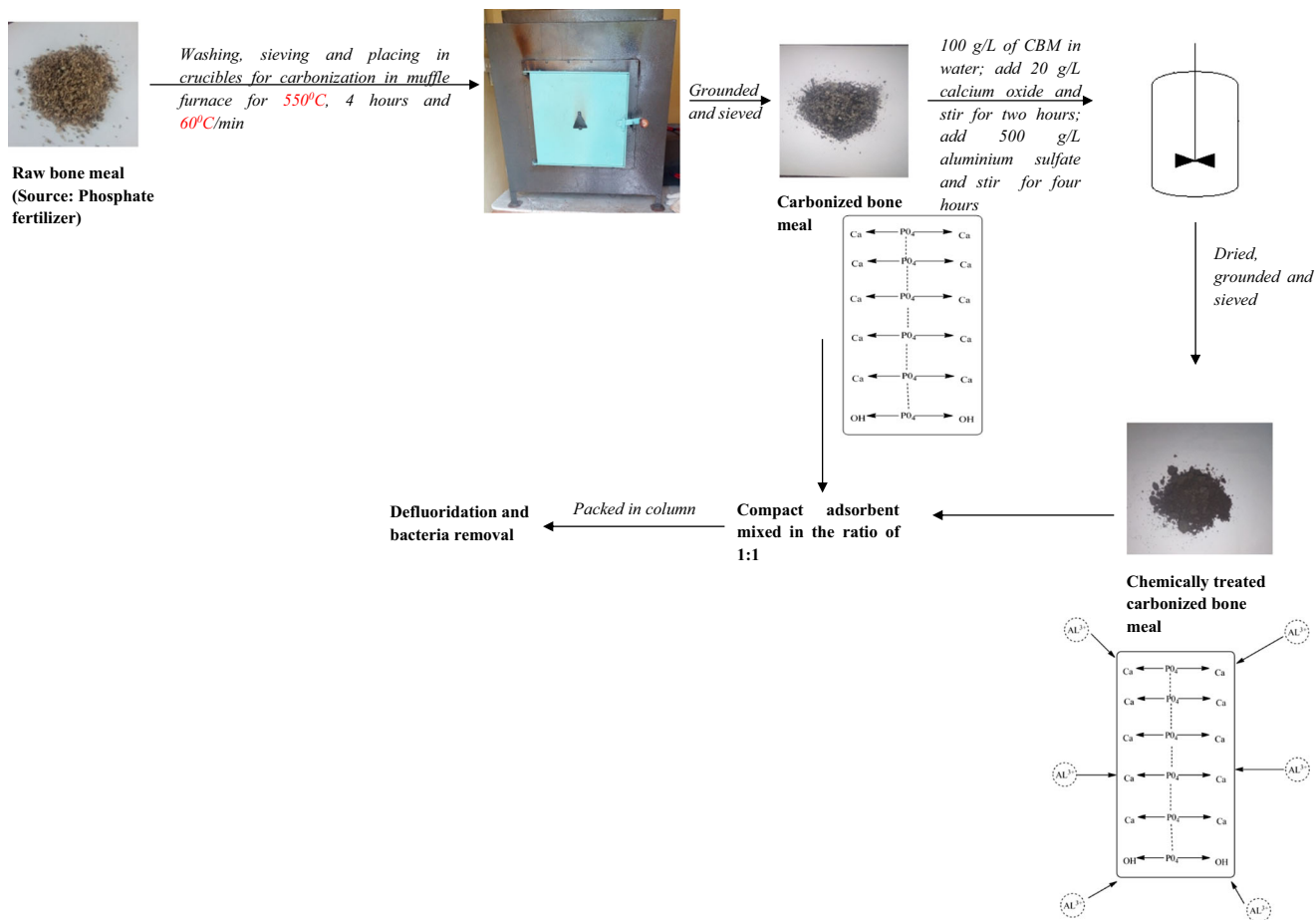


Fig. 1 Scheme for production of chemically treated carbonized bone meal and its application

**Effect of coexisting ions**

Effect of different coexisting anions, like sulfate, phosphate, carbonate, nitrate, and chloride along with cations, like calcium and aluminum on defluoridation capacity of CTBM, was observed. These ions having concentration in the range 50 to 500 mg/L were mixed with 10 mg/L fluoride in synthetic aqueous solution. Temperature in the shaker was maintained at 30 °C with speed 150 rpm at the optimum pH and adsorbent concentration.

**Desorption study**

One gram per liter of CTBM was exposed to a solution having 10 mg/L fluoride concentration for 24 h at 30 °C with 150-rpm shaking speed. Fluoride concentration in the residual filtrate was measured after equilibration after separating fluoride-adsorbed CTBM by a filter cloth. Fluoride-adsorbed CTBM was transferred to 100 mL water and the pH was varied from 2 to 12. Again, equilibration was performed for 10 h under above operating conditions. After this, fluoride concentration in desorption medium was measured. Amount of fluoride

adsorbed and desorbed during each cycle was calculated by Eq. (1). The experiments were repeated for three cycles.

**Adsorption kinetics**

Solution having 10 mg/L fluoride concentration was prepared and 1 g/L of CTBM was loaded at 150-rpm shaker speed. Fluoride concentration in the residual filtrate was measured after different time intervals. Concentration profiles were generated at three different temperatures, 30, 40, and 50 °C. Kinetic data was modeled using shrinking core model (Jena et al. 2003). Detailed discussions are given in Supplementary Section S3.

**Fixed-bed adsorption study**

CTBM was powdered and sieved to 0.1-mm diameter and it was packed in a perspex column having a diameter of 3 cm. Due to its small particle size, CTBM offered high resistance for fluid flow through the packed column. Therefore, it was mixed with CBM having a particle diameter of 0.5 mm. Net weight of the adsorbent, i.e., CTBM and CBM, was kept fixed at 100 g. Effects of CBM-to-



CTBM weight ratio (30:70, 50:50, 70:30), flow rate (30, 40, and 50 mL/min), and feed concentration (5, 10, and 15 mg/L) on the effluent fluoride concentration were noted. Calculations of various fixed-bed parameters are given in Supplementary Section S4. Modeling of the column run data was performed using pore diffusion-adsorption model. Model constants were evaluated by minimizing the error between predicted and experimental concentration profiles. Relevant model equations and their solution strategy are discussed in Supplementary Section S5.

### Fluoride-contaminated groundwater solution

Contaminated groundwater sample was obtained from Kamaladanga Raipara colony, Bankura city (GPS location: 23.25° N, 87.07° E), West Bengal, India. Defluoridation capacity of the column packed with CTBM and CBM was obtained. Column conditions were 50:50 (CTBM: CBM) and 60-mL/min flow rate. Concentration of different ions present both in feed and in filtrate was also measured.

### Antibacterial property of CBM and CTBM

Antibacterial efficiency of CBM and CTBM was investigated using the coliform bacteria, i.e., *Escherichia coli* (ATCC 10536). Bacteria cells were cultured overnight in a flask containing 10 mL of *E. coli* broth at 37 °C. The cells were harvested and re-suspended in phosphate buffer solution (0.01 M, pH 7). The post-treatment cellular alteration of bacteria was observed by direct microscopic observation by FESEM and fluorescent microscope (Zeiss Axioscope A1, Carl Zeiss, Goettingen, Germany). For FESEM, 10 mL of bacteria solution was treated with either 0.2 g CBM or CTBM. Afterwards, the bacteria sample was incubated on a shaker at 150 rpm for 24 h at 37 °C. The cells were then harvested and dehydrated in 25, 50, 75, and 100% ethanol (Mukherjee and De 2015). The morphology of bacteria prior and post-treatment was studied and compared. For fluorescence image, bacteria cells were harvested and washed three times with phosphate buffer solution (PBS). Thereafter, cells were stained with 10 µL fluorescein isothiocyanate (FITC, Sigma, USA) and incubated in dark at 37 °C for 2 h. The excess dye was removed by washing the cells with PBS (Mukherjee and De 2017).

## Results and discussions

### Optimum conditions for preparation of adsorbent

Effect of carbonization conditions on the defluoridation capacities was observed and reported in Table S1(a). Yield

percentage of each sample after partial carbonization was calculated as,

$$yield = \left( \frac{A-B}{A} \right) \times 100\% \quad (2)$$

where *A* and *B* are the weight of RBM and CBM, respectively. It was observed from this table that the yield percentage decreased with carbonization temperature due to conversion of carbon of RBM to carbon dioxide gas. For example, the yield percentage of sample A (carbonized at 300 °C) is 74% while that of sample E (carbonized at 800 °C) is 40%. However, with increase in carbonization temperature, surface area of the sample increases along with its defluoridation capacity. For example, the surface area of sample A is 75 m<sup>2</sup>/g and it increases to 97.2 m<sup>2</sup>/g for sample C (carbonized at 550 °C). Defluoridation capacities of sample A and C are 1.2 and 8.3 mg/g, respectively. However, with further increase in temperature, surface area and fluoride uptake capacity decrease. This is observed in the case of sample D (carbonized at 700 °C) and E (carbonized at 800 °C) having reduced surface area of 80 and 72 m<sup>2</sup>/g, respectively. Samples D and E have a defluoridation capacity of 3.2 and 3 mg/g. These observations confirm that the surface area of the prepared carbonized adsorbents affects fluoride removal capacity. Time of carbonization also has effect on extent of defluoridation. For example, samples prepared at 550 °C for 2 h (sample F) have 96-m<sup>2</sup>/g surface area and 5-mg/g defluoridation capacity, while samples carbonized for longer duration, i.e., 4 h (sample G), has 104-m<sup>2</sup>/g surface area and 12.5-mg/g capacity. Decrease in surface area (95 m<sup>2</sup>/g) with defluoridation capacity (8.3 mg/g) is observed in the case of sample H. Structural modification of apatite in CBM occurs with time and temperature playing a key role in variation of surface area and defluoridation capacity (Rojas-Mayorga et al. 2013). Sample G (partially carbonized at 550 °C for 4 h), having the highest surface area and defluoridation capacity, is selected for further chemical treatment to enhance its performance. Chemical treatment by different aluminum and calcium compounds was performed. Suitable combination of chemicals was selected on the basis of maximum fluoride removal capacity of the final product. For example, when calcium chloride and aluminum chloride (Tchomgui-Kamga et al. 2010a, b) were used as impregnating chemicals, the uptake capacity was 19 mg/g (refer to Table S1b). The capacity decreased to 15 mg/g in the case of alum treatment. It was further decreased to 13 mg/g in the case of aluminum sulfate and sodium hydroxide treatment (precipitate of aluminum hydroxide occurs on the surface of precursor by this method) (Ganvir and Das 2011). The first pair of chemicals has an inefficient coating of aluminum compounds on the surface of the precursor, CBM. Alum treatment of bone char does not render aluminum coating. Stability of aluminum hydroxide deposits on the surface of CBM is not strong

(Nigussie et al. 2007). However, after treatment by aluminum sulfate and calcium oxide, the uptake capacity was observed to be 26 mg/g (see Table S1b). When aluminum sulfate is dissolved in water, the solution becomes acidic and hence there is high probability of calcium leaching from the CBM (Zhang et al. 2008). Therefore, calcium oxide is added to the solution at the first instance, to offer a reverse concentration gradient to prevent calcium leaching. It also makes the treatment pH basic, resulting in precipitation of aluminum hydroxide on the CBM surface. The routes of chemical treatment have significance in determining the uptake capacity. For example, it was observed from Table S1(b) that impregnation of chemicals to raw bone meal followed by carbonization yields a comparatively lower adsorption capacity (10 mg/g) than impregnation of chemicals to CBM. Aluminum may increase heat conduction on the raw bone meal surface, which in turn degrades the apatite structure and hence reduces the uptake capacity (Yu et al. 2013). However, in the case of CBM, this is not observed. Hence, the final material had calcium in the apatite structure and aluminum coating on the surface providing a synergistic effect on fluoride removal (Nie et al. 2012). It was observed from Table 1 that the uptake capacity was increased from 26 to 102 mg/g as the concentration of aluminum is increased in the treatment step. This is due to an increase in aluminum hydroxide coating on CBM surface at higher concentration. However, on further increase of concentration, change in uptake capacity is insignificant due to saturation of coating on the surface. When concentration of calcium oxide is increased in the treatment medium, the uptake capacity increases to

150 mg/g. Increase in the reverse concentration gradient arrests leaching of calcium from the CBM thereby increasing fluoride uptake capacity. However, the uptake capacity was reduced to 66 mg/g when the calcium oxide concentration was decreased to 5 g/L, keeping aluminum sulfate fixed at 500 g/L. Precipitation of calcium hydroxide occurs at higher calcium oxide loading in water, lowering the concentration gradient and initiating leaching, thereby decreasing the fluoride uptake capacity. For example, the uptake capacity decreases to 114 mg/g when the calcium oxide concentration reaches 50 g/L. Therefore, the material used for further studies was prepared with 500 g/L aluminum sulfate and 15 g/L of calcium oxide, as it has the highest fluoride uptake capacity.

## Characterization

Various characterization techniques (mentioned in “Adsorbent characterization”) are shown in Fig. 2. Morphological analysis, as performed by scanning electron microscopy, suggests that the surface of CBM (see Fig. 2(a)) is smoother than that of CTBM at the same magnification (refer to Fig. 2(b)). Also, it is quite evident from this figure that deposit of aluminum hydroxide occurs on the surface of the CTBM as a result of chemical treatment (Ganvir and Das 2011). The elemental analysis, shown in Table 2, clearly suggests the presence of aluminum in CTBM. Conductivity of the treated stream increases from 1520 to 2500  $\mu\text{S}/\text{cm}$  (see Table 2), indicating presence of ionic elements, like aluminum. Presence of calcium is common in the apatite structure of both CBM and CTBM and it is also confirmed by the elemental analysis (Rojas-Mayorga et al. 2013). Sharp differences in adsorption capacities are observed between the CBM and CTBM due to the coated aluminum on the latter, though the surface area of the two adsorbents remains almost same (see Table 2).

Crystal structure of the prepared adsorbent is evident from the TEM images, as shown in Fig. 2(c). Sharp rod-like structures of deposits is observed on the surface of the adsorbents. Also, presence of worm-like pores is confirmed on the surface of the adsorbent by TEM images. Similar observations were recorded in the case of synthesized boehmite AlOOH nanotubes (Kuang et al. 2003). The interlayer distance between the lattice fringes of the rod-like structure is 0.4 nm, corresponding to aluminum hydroxides (Kuang et al. 2003).

XRD images, from Fig. 2(d), show the transformation of broad and low intense peaks of CBM to narrow and strongly intense peaks of CTBM. For example, broad hydroxylapatite peak at diffraction angle of  $\theta = 30^\circ$  of CBM (JCPDS, card no. 9-432) is narrowed in CTBM. This peak may represent calcium oxide along with a weak diffraction peak at  $\theta = 24^\circ$  (Tchomgui-Kamga et al. 2010a, b). Narrowness of the peaks increases the crystallinity, improving the fluoride uptake capacity (Rojas-Mayorga et al. 2013). It may also be observed that peaks corresponding to boehmite are present at  $\theta = 22^\circ$

**Table 1** Variation of fluoride uptake capacity with aluminum sulfate and calcium oxide dosages in preparation medium

Aluminium sulfate dosage (g/L)	Calcium oxide dosage (g/L)	Maximum adsorption capacity (mg/g)	Heat of sorption (L/g)
Aluminium sulfate dosage variation			
50	10	26	0.1
100	10	57	0.1
200	10	59	0.1
300	10	72	0.1
500	10	102	0.1
700	10	100	0.1
1000	10	105	0.01
Optimization of calcium oxide dosage			
500	5	66	0.04
500	15	150	0.04
500	20	124	0.02
500	30	113	0.02
500	50	114	0.03

Italics represent the dosages at which maximum defluoridation capacity has been obtained

and  $\theta = 32^\circ$  (Tchomgui-Kamga et al. 2010a, b). Weak diffraction peaks at  $\theta = 44^\circ$  and  $52^\circ$  suggest presence of aluminum hydroxide (Wang et al. 2009).

Thermal analysis of the CTBM is shown in Fig. 2(e). Three regions of weight loss are observed from this figure. The first region, i.e., weight loss from 25 to 110 °C, represents moisture loss (approximately 10% weight loss) from the material. The second region from 110 to 200 °C represents the loss of hydroxyl groups from aluminum and calcium components of the adsorbents (Kim et al. 2008). The loss in mass is 20%. Finally, a steady decrease of 6% mass is noted from 200 to 700 °C. This happens due to slow dehydroxylation (Kim et al. 2008).

Chemical treatment of CBM imparts aluminum and calcium oxide groups within the adsorbent. As shown in Fig. 2(f), transmittance corresponding to 3544 and 3401  $\text{cm}^{-1}$  wave number represents hydroxyl group stretching of calcium hydroxide (Granados et al. 2007). Frequencies between 2239 and 2115  $\text{cm}^{-1}$  confirm the presence of methoxy and medial alkyne (Siesler et al. 2008). Transmittance recorded at 1404  $\text{cm}^{-1}$  can be assigned to asymmetric stretching of O–C–O bonds of carbonate groups at the surface of calcium oxide. Presence of phosphate group is confirmed by the transmittance at 1015  $\text{cm}^{-1}$  (Granados et al. 2007; Siesler et al. 2008). Frequency between 1685 and 1404  $\text{cm}^{-1}$  suggests the presence of purines. Shift in stretching frequencies of  $\alpha$ -calcium pyrophosphate is observed from 559 to 669  $\text{cm}^{-1}$  due to chemical treatment. Impregnated aluminum groups can be found within the synthesized adsorbent in the form of  $\text{AlO}_6$  and Al–OH indicated by the stretching frequencies at 602, 1107, and 1621  $\text{cm}^{-1}$  (Du et al. 2009).

### Antibacterial property

Fresh cells of *E. coli* before treatment are presented in Fig. 3a. The untreated cells of bacteria have the normal structure (length  $1.5 \pm 0.5 \mu\text{m}$ ; thickness  $0.5 \pm 0.1 \mu\text{m}$ ), as expected. Morphological alteration of bacteria is evident after treatment with CBM and CTBM. While exposed to CBM, bacteria cells were found twisted and several pits appeared in their cell wall. Such disruption was more pronounced after treating with CTBM. It is evident from Fig. 3b, c that bacteria cells were shrunk with appearance of several pores within the wall, indicating rupture of cell wall, leading to death of cultured bacteria.

The fluorescence microscopy images of untreated bacteria are presented in Fig. 3d. It should be noted that FITC dye could pass through the intact membrane and bind to DNA, emitting green fluorescence. The viability of fresh bacteria cells was clear by bright-green fluorescence. After the treatment with CBM, the viable count of bacteria was reduced, as evident by less number of green dots (see Fig. 3e). However, significant loss of viability was noticed after treatment with CTBM, indicating its antibacterial property (see Fig. 3f). Nevertheless, it is interesting to note that the chemical treatment results in enhancing surface area of the particles up to

110  $\text{m}^2/\text{g}$ . In addition, the positive surface potential of CTBM also increases after the subsequent treatment. The zero point charge ( $\text{pH}_{\text{ZPC}}$ ) of CTBM was 6.7, indicating they have negative surface potential beyond this pH. Thus, strong electrostatic interaction between the CTBM particles and bacteria promotes the cellular damage, exhibiting efficient antibacterial property (Delgadillo-Velasco et al. 2017).

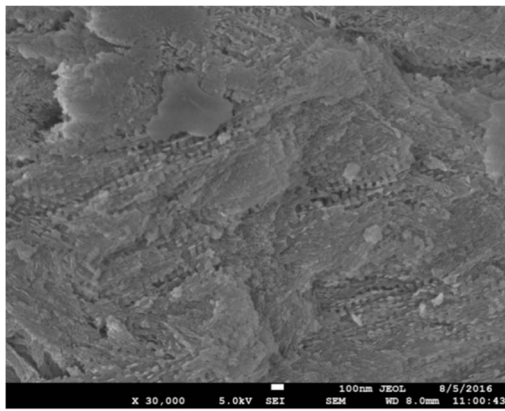
### Fluoride uptake capacity in batch study

Batch studies were conducted to obtain the optimum process conditions, effect of temperature, time, and coexisting ions on the fluoride uptake capacity. Variation of adsorption capacity in regeneration cycles is also conducted in batch mode.

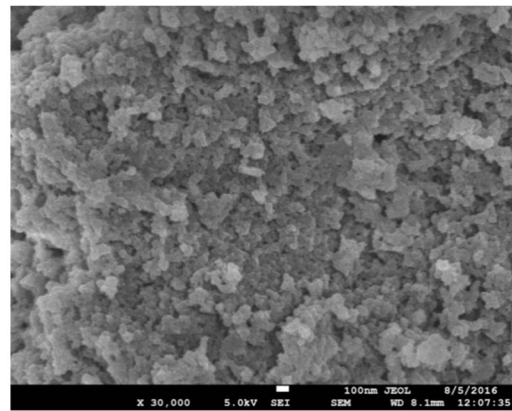
Effect of operating conditions, i.e., pH, size, and adsorbent concentration on the fluoride uptake capacity, is shown in Fig. 4(a). It is observed from this figure that pH of the feed solution controls the uptake capacity by the adsorbent. For example, the residual filtrate concentration after uptake is 0.04 mg/L at highly acidic pH, i.e., pH 2. At pH 6.1, fluoride concentration in the residual filtrate increases to 0.3 mg/L, which is below the permissible level (1.5 mg/L). The isoelectric pH or  $\text{pH}_{\text{ZPC}}$  of CTBM (6.7) has an important role in tuning the surface charge of the material. As the pH of the feed solution is lower than the isoelectric pH, surface of CTBM becomes positive, attracting negatively charged fluoride ions, thereby facilitating adsorption. The reverse is being observed at higher pH (Chatterjee et al. 2017). Due to the sustained efficiency until pH 6.1, it is selected as the operating pH. Uptake capacity also depends on the size of the adsorbent, which is clearly observed from this figure. The residual filtrate concentration decreases from 0.3 to 0.1 mg/L, when the size of the particle is decreased from 0.5 to 0.15 mm. For smaller adsorbents, specific surface area increases intensifying the adsorbent-adsorbate interaction (Tchomgui-Kamga et al. 2010a, b; Chatterjee and De 2016). Another significant factor that controls the fluoride uptake capacity is the adsorbent concentration during batch treatment. It can be observed from this figure that the residual filtrate concentration is 8.65 mg/L (fluoride feed concentration of 10 mg/L) when the adsorbent concentration is 0.1 g/L. However, the filtrate concentration decreases to 0.2 mg/L at an adsorbent concentration of 5 g/L. This is due to the higher number of active sites at enhanced adsorbent loading in the feed solution (Tchomgui-Kamga et al. 2010a, b). However, further increase in active sites leads to saturation of uptake capacity at higher adsorbent dose. This is quite evident from the figure, as the residual filtrate concentration does not decrease below 0.2 mg/L even at 20 g/L of adsorbent concentration.

Effect of temperature on fluoride uptake capacity is shown in Fig. 4(b). It is observed from this figure that the uptake capacity of fluoride by CTBM increases with the equilibrium concentration, due to enhanced driving force. For example,

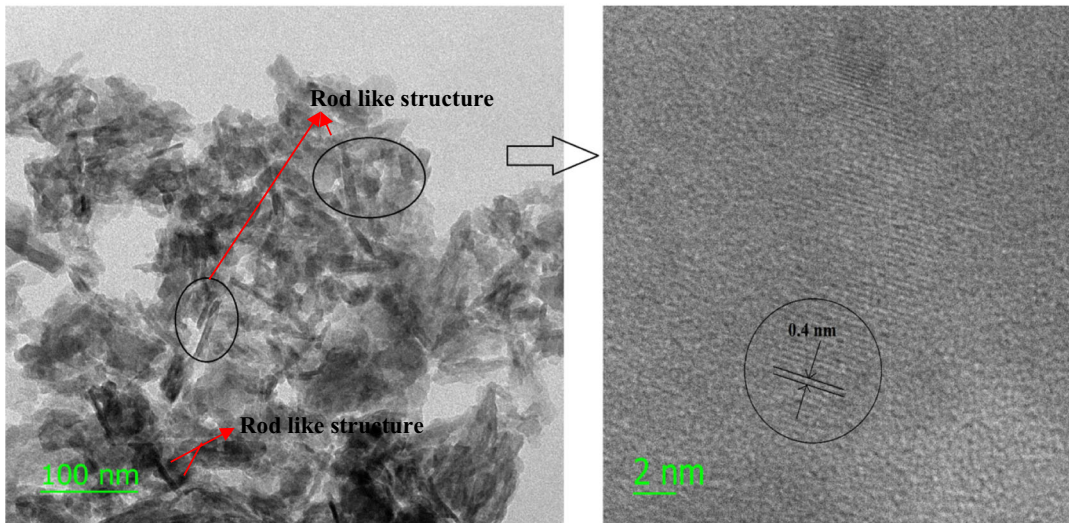




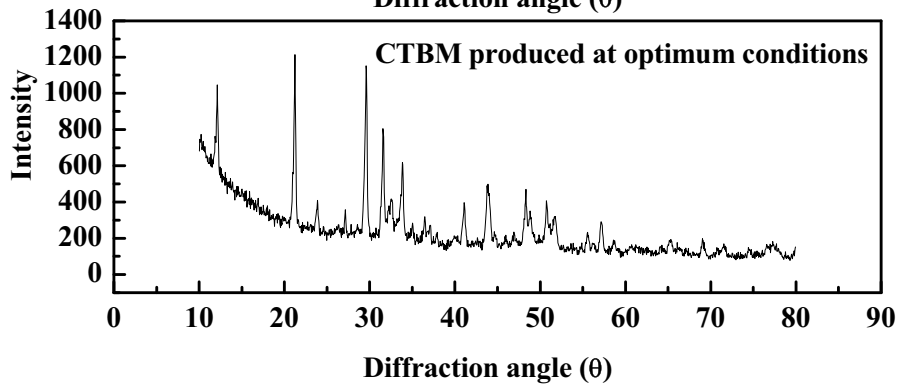
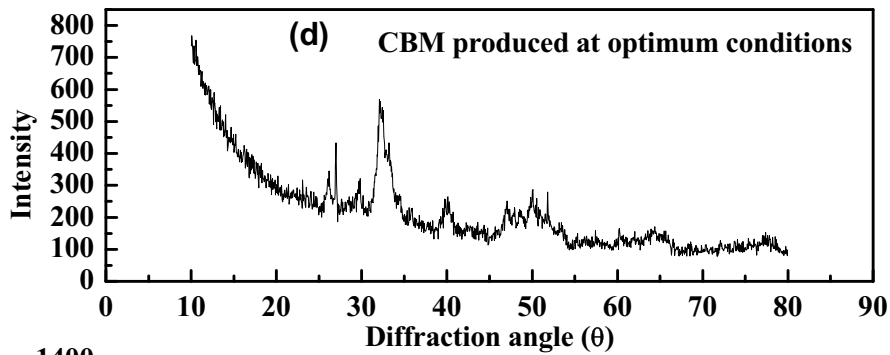
(a)



(b)



(c)





◀ **Fig. 2** SEM images of (a) CBM and (b) CTBM. (c) TEM image of CTBM at different resolution. (d) X-ray diffractograms of CBM and chemically treated CBM. (e) TGA of chemically treated CBM. (f) FTIR spectra of chemically treated CBM before and after fluoride adsorption

the uptake capacity is 25 mg/g at an equilibrium concentration of 10 mg/L; this increases to 142 mg/g when the equilibrium concentration is increased 100 times, i.e., 1000 mg/L. Also, uptake capacity decreases with temperature. For example, the uptake capacity substantially decreases from 25 mg/g at 30 °C to 12 mg/g at 40 °C when the equilibrium concentration is 10 mg/L. At even higher temperature, i.e., 50 °C, uptake capacity is 10 mg/g at the same equilibrium concentration. Decrease in uptake capacity with temperature occurs due to lowering of surface tension of the adsorbent at higher temperature, thereby attracting less fluoride laden water molecules (Wu et al. 2015). Weakening of adsorptive forces, like Van der Waals interaction at higher temperature, is another reason (Wu et al. 2015). Similar behavior of exothermic adsorption was observed in the case of fluoride adsorption onto synthetic siderite and cerium-impregnated fibrous protein (Liu et al. 2010; Deng and Yu 2012). The data sets have been fitted to various

isotherm models (discussed in Supplementary Section S1) and the results are shown in Table S2. Monolayer adsorption capacity of 150 mg/g is predicted from the Langmuir isotherm. The same uptake capacity predicted by Freundlich and D-R isotherm is 32.9 and 191 mg/g, respectively. The correlation coefficient is the highest for Langmuir isotherm, indicating uptake of fluoride by CTBM is monolayer adsorption process. The separation factor from this isotherm lies well below 1 (0.05–0.8) for all the concerned temperatures, suggesting favorable adsorption of fluoride onto CTBM. This is also corroborated by the Freundlich isotherm constant ( $n$ ) that lies below 10 (4.3–2.9) at all temperatures. The factor  $\frac{1}{n}$  is a measurement of the heterogeneity of the adsorbent and it increases with temperature (0.23 at 30 °C, 0.26 at 40 °C, and 0.34 at 50 °C), making the system more heterogeneous at lower temperature. The mean free energy value (from DR isotherm) for the system at different temperatures lies between 8 and 16 kJ/mol, indicating the uptake as chemisorption in nature. Value of  $n_n$ , i.e., number of fluoride ion bound per active sites of CTBM from the statistical three-parameter isotherm model (Hill isotherm), provides mechanistic insight to adsorption. For example, if the value of this parameter is greater than unity, then adsorption is multi-ion process. Contrary to this, adsorption is a multi-anchorage process (fluoride ions adsorbed in parallel positions on CTBM surface), when its value is less than unity. However, the mechanism becomes mono-anchorage, i.e., the fluoride ions are adsorbed at perpendicular position to the active sites of CTBM, when its value is one (Sellaoui et al. 2017a, b; Sellaoui et al. 2016). It can be observed from Table S2 that number of fluoride ions per adsorption sites of CTBM is one at 30 °C, which marginally increases with temperature (1.1 and 1.2 at 40 and 50 °C, respectively). Hence, it can be inferred that the uptake mechanism is mono-anchorage at lower temperature, which gradually changes to multi-ion process at higher temperature. This happens due to thermal agitation at higher temperature when the mobility of fluoride ions increases and more fluoride ions are attached to the active sites. However, this is not the same for the density of receptor sites ( $N_m$ ) and density of receptor sites decreases with temperature. For example, the value of  $N_m$  is 148 mg/g at 30 °C and decreases to 92.3 mg/g at 50 °C. As discussed earlier, increase in temperature results in weakening of Van der Waals adsorptive forces as well as surface tension of adsorbent thereby reducing  $N_m$  and uptake capacity,  $Q_{sat}$ . Results of adsorption thermodynamics (calculation of various thermodynamic parameters has been discussed in Supplementary Section S2) are also reported (see Table S3). Negative value of Gibbs free energy (– 16 kJ/mol) confirms the spontaneity of fluoride adsorption on the CTBM surface. Enthalpy change is negative (– 44.8 kJ/mol) and its absolute value is higher than 40 kJ/mol. This proves the exothermic nature of adsorption and chemisorption as uptake mechanism.

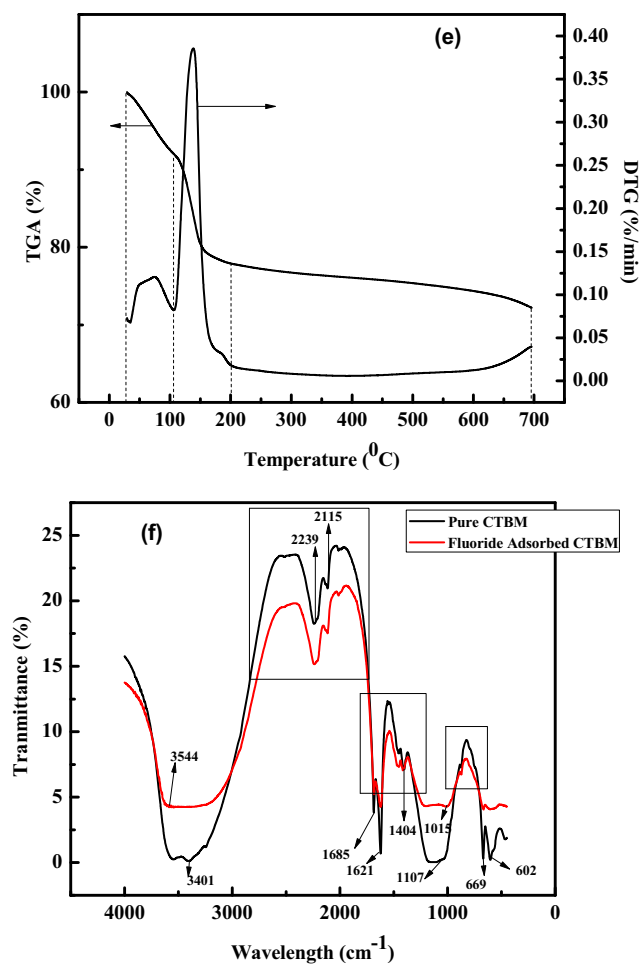


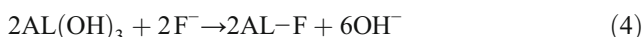
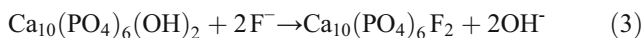
Fig. 2 (continued)

**Table 2** Comparison of properties between CBM and CTBM (produced at optimum conditions)

Parameters	CBM	CTBM
Particle size (mm)	0.4-0.6	0.1-0.3
Surface area (m <sup>2</sup> /g)	58	110
Pore volume (mL/g)	0.1	0.3
Bulk density (kg/m <sup>3</sup> )	900	980
Particle density (kg/m <sup>3</sup> )	2000	1428
Material density (kg/m <sup>3</sup> )	2700	2300
Particle porosity	0.3	0.4
Bed porosity	0.5	0.6
pH <sub>ZPC</sub>	7.6	6.7
Conductivity (1:5 ratio of adsorbent and distilled water) (μs/cm)	1520	2500
pH (1:5 ratio of adsorbent and distilled water)	6.8	5.3
Maximum adsorption capacity of fluoride (mg/g) at 303 K	14 (0.1 mm particle size) and 12 (0.5 mm particle size)	150
Elemental analysis	Carbon: 10.2	Carbon: 27.8
	Nitrogen: 3.4	Nitrogen: 6.2
	Oxygen: 45.4	Oxygen: 38.2
	Phosphorus: 15	Aluminium: 2.4
	Calcium: 25.5	Phosphorus: 1
		Sulphur: 13.2
	Calcium: 11.2	

The entropy change is 94 J/mol K indicating increased rapidity of fluoride ions at the interface favoring adsorption (Chatterjee and De 2016; Foo and Hameed 2010).

Interaction of fluoride with the chemical species in CTBM (Tchomgui-Kamga et al. 2010a, b; Rojas-Mayorga et al. 2013), i.e., calcium and aluminum, results in its removal. Uptake mechanism can be represented by ion exchange as follows:

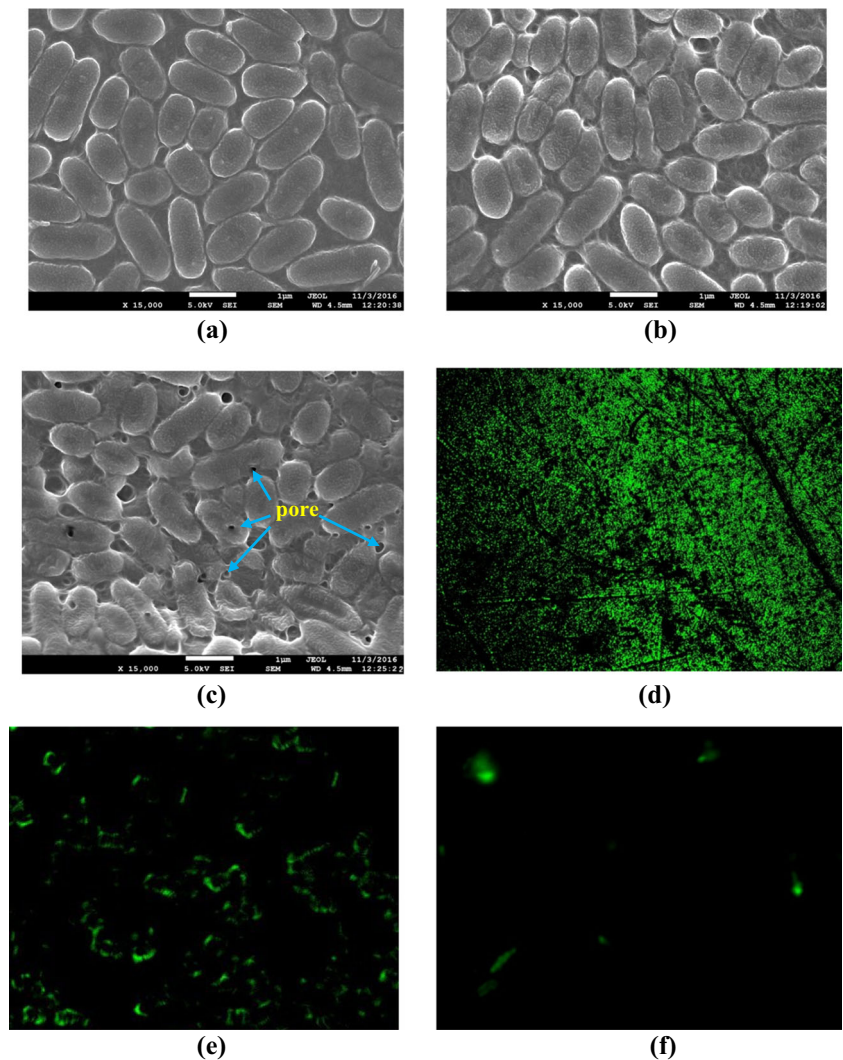


Effect of time on the residual fluoride concentration is shown in Fig. 4(c). It is observed that the residual filtrate concentration decreases with time. For example, the residual filtrate concentration decreases to 0.13 mg/L from 10 mg/L within the first hour. With increase in interaction time, i.e., 24 h, the residual filtrate concentration reaches equilibrium to 0.04 mg/L. It is also observed that the residual fluoride concentration in the filtrate increases with temperature. This is exactly in line with the exothermic adsorption effect, as discussed earlier. Data of kinetic experiments were compared with the predicted values from shrinking core model (discussed in Supplementary Section S3) (Chatterjee and De 2016; Chatterjee et al. 2017). The model constants are reported in Table S4. Effective diffusivity of fluoride within the

pores of CTBM remains invariant with temperature. For example, the effective diffusivity is  $5.8 \times 10^{-12}$  m<sup>2</sup>/s at 30 °C; at 50 °C, it is  $6.2 \times 10^{-12}$  m<sup>2</sup>/s. However, the mass transfer coefficient of fluoride decreases with temperature. For example, the mass transfer coefficient decreases from  $9 \times 10^{-4}$  m/s at 30 °C to  $8.5 \times 10^{-4}$  m/s at 50 °C, leading to reduction in uptake capacity. Biot number of the CTBM-fluoride system is quite high (in the range of  $10^3$ ) signifying pore diffusion as dominant mechanism. Tortuosity factor, which is the ratio of bulk to effective diffusivity, lies in the range of 1–10, indicating CTBM is a porous adsorbent. Radius of concentration front is a measure of the extent of adsorption. Reduction of radius is more at lower temperature and it is in line with exothermic adsorption in this case.

Effect of different contaminating ions, coexisting with fluoride in groundwater, has been observed and is shown in Fig. 4(e). Cations, like calcium and aluminum, do not have adverse effect on the uptake capacity of fluoride, as observed from this figure. Removal percentage remains 100% at lower concentration, i.e., 50 mg/L and even at higher concentration, i.e., 500 mg/L. Anions, like chloride, nitrate, sulfate, carbonate, and phosphate, essentially compete with fluoride for the active sites in CTBM. For example, the adsorption percentage decreases to 95 and 88% when the concentration of chloride in the synthetic solution is 50 and 500 mg/L, respectively. Similarly, adsorption capacity decreases to 80, 75, and 62% in the case of carbonate, nitrate, and sulfate, respectively, at a concentration of 500 mg/L. Maximum hindrance is offered by

**Fig. 3** Antibacterial property of CTBM highlighting the SEM images of **a** bacterial cell, **b** bacterial cell treated by CBM, and **c** bacterial cell treated by CTBM. Fluorescence images of **d** bacterial cell, **e** bacterial cell treated by CBM, and **f** bacterial cell treated by CTBM



phosphate as the adsorption of fluoride drops to 90 and 58% at concentrations of 50 and 500 mg/L. Competitive adsorption significantly depends on the number of negative charge carried by that ion and its ionic mass (Njoku 2014).

Variation of adsorbed and desorbed amount of fluoride with regeneration cycles is shown in Fig. 4(f). It is observed from this figure that the uptake capacity of fluoride is 2.2 mg/g, when fluoride feed concentration is 10 mg/L. As the fluoride-loaded sorbent is added to 0.1 (N) sodium hydroxide solutions, 1.5 mg/g of fluoride is desorbed. Hydroxyl radicals are generated at alkaline pH decreasing the bond energy of fluoride-encapsulated active sites, thereby releasing fluoride (Tang et al. 2009). The amount of fluoride adsorbed and desorbed during each cycle is not equal. This is due to chemical adsorption of fluoride species by aluminum and calcium components of CTBM. It is also observed from this figure that the adsorption percentage decreases successively after each cycle. For example, the adsorption percentage decreases by 18% (1.8 mg/g) and 31% (1.5 mg/g) in the second and third regeneration cycles, respectively. This

happens due to unavailability of some active sites during uptake, binding strongly the fluoride ions.

**Dynamic column study**

Batch study under stirring provides an ideal mixing between adsorbate and adsorbent. However, for real-life applications, dynamic equilibrium in column mode needs to be studied. Therefore, experiments were performed and pore diffusion-adsorption model (developed from fundamental convective-diffusive equation) was used for simulation (Singha et al. 2012). Detailed description of model equations has been discussed in Supplementary Section S5. Numerical solution strategy of the equations describing the model is shown in Fig. S1. The major advantages of this model includes intrinsic model constants, flexibility in engineering design of adsorbent bed, and capability of incorporating fluctuations in the breakthrough behavior during abnormality of input conditions. In this case, effect of adsorbent quantity, flow rate, and inlet feed concentration on the dynamic equilibrium capacity has been

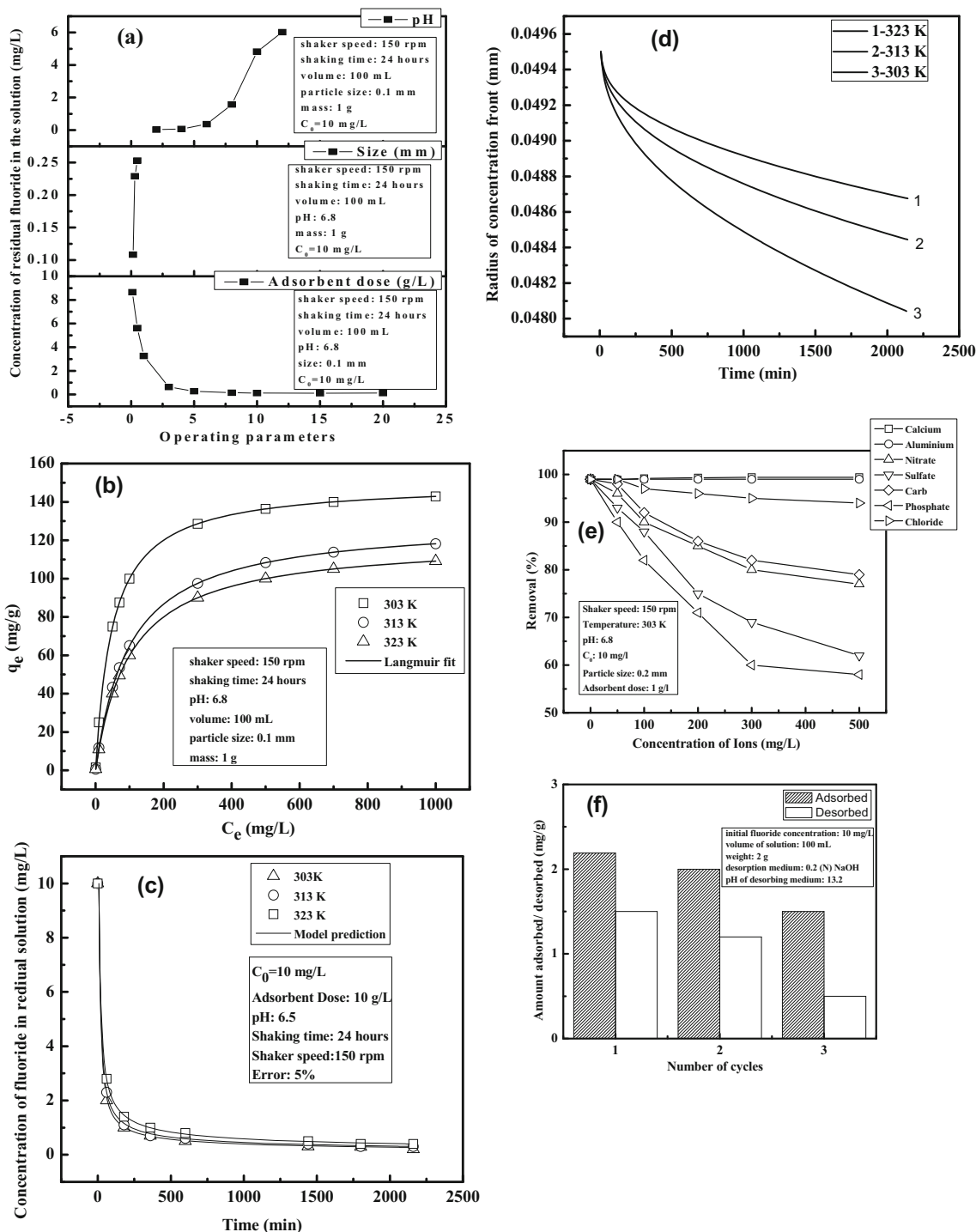


**Fig. 4** (a) Effect of operating conditions (dose, pH, and size) on removal capacity. (b) Adsorption isotherm at different temperatures. (c) Effect of temperature on uptake of fluoride by chemically treated CBM and

simulated curve. (d) Profile of radius of concentration front at different temperatures. (e) Effect of competing co-ions. (f) Adsorption-desorption cycle

observed and is shown in Fig. 5(a, b, c). It was observed that the breakthrough time (time required for the filtrate concentration to reach the allowable limit of fluoride in water, 1.5 mg/L) and exhaustion time (time required for the filtrate concentration to reach 90% of the inlet feed concentration) increased

with higher CTBM loading in the mixed adsorbent. As observed from Fig. 5(a), the breakthrough curve shifts towards the right, when the amount of CTBM is increased in the mixed adsorbent. The breakthrough and exhaustion time for a 30:70 (CTBM:CBM) column were 24 h (number of bed volumes,



340) and 65 h (number of bed volumes, 920), respectively (see Table S5). These increase to 49 h (number of bed volumes, 462) and 95 h (number of bed volumes, 896), when the amount of CTBM is increased (70:30). Model predictions show that the breakthrough time in the case of 30:70 column is 35 and 65 h, respectively. While for the 70:30 column, the predicted breakthrough and exhaustion were 51 h (number of bed volumes, 480) and 88 h (number of bed volumes, 829). It has been observed previously that the shorter beds have lower adsorption capacity due to less quantity of adsorbents. Column with higher loading of CTBM has higher breakthrough than the one with lesser loading. It may also be pointed out that mass transfer zone increases from 11.4 to 13.1 cm (see Table S5) due to higher weight percentage of CTBM and hence delayed saturation is observed (Sulaymon et al. 2009).

It may be observed from Fig. 5(b) that the increase in flow rate results in shorter breakthrough. For example, in a 50:50 column, with 5-mg/L inlet fluoride concentration, the breakthrough and exhaustion time were 34 h (number of bed volumes, 433) and 90 h (number of bed volumes, 1146), respectively, when the flow rate is maintained at 30 mL/min. As the flow rate is increased to 50 mL/min, the exhaustion and breakthrough time decrease to 14 h (number of bed volumes, 297) and 38 h (number of bed volumes, 806) (see Table S5). The predicted breakthrough and exhaustion time in the case of 50:50 column were 48 h (number of bed volumes, 611) and 90 h (number of bed volumes, 1146), for 30-mL/min flow rate, while for 50 mL/min, the predicted times were 17 h (number of bed volumes, 360) and 42 h (number of bed volumes, 890). Due to shorter adsorbate-adsorbent interaction, the breakthrough curve shifts towards the left (Sulaymon et al. 2009). It may also be observed that the dynamic uptake capacity is decreased from 4.2 to 3 mg/g with flow rates (see Table S5) due to ineffective mass transfer, resulting in shorter saturation time.

Increase in inlet concentration decreases the saturation time (refer to Fig. 5(c)). For example, the breakthrough and exhaustion time for 50:50 column at 30-mL/min flow rate were 34 h (number of bed volumes, 433) and 90 h (number of bed volumes, 1146) as the inlet concentration of fluoride in synthetic solution is 5 mg/L. But the breakthrough and exhaustion time decrease to 10 h (number of bed volumes, 127) and 41 h (number of bed volumes, 523) as concentration increases to 15 mg/L, keeping all other process conditions the same. The predicted breakthrough and exhaustion time in the case of 5 mg/L were 48 h (number of bed volumes, 611) and 90 h (number of bed volumes, 1146), while they were 11 h (number of bed volumes, 140) and 39 h (number of bed volumes, 497), when the concentration is increased to 15 mg/L. At lower concentration, delayed breakthrough is observed due to lower driving force (Sulaymon et al. 2009). However, increased inlet concentration leads to higher driving forces resulting in rapid saturation. For example, the separation percentage in the case

of 5-mg/L inlet fluoride concentration is 49%, which decreases to 38%, as the concentration increases to 15 mg/L.

Axial dispersion and pore diffusion coefficient (evaluated by minimizing differences between experimental and simulated profiles) were  $9 \times 10^{-11}$  and  $1.1 \times 10^{-10}$  m<sup>2</sup>/s, respectively (see Table S6). It is clearly observed that the pore diffusion constant is higher than the axial dispersion constant, thereby suggesting removal occurs by diffusion of fluoride ions through the pores of CTBM and CBM rather than external mass transfer on the outer surface. Mass transfer coefficient is seen to vary inversely with bed height, thereby leading to delayed breakthrough at increasing bed depth. For example, the mass transfer coefficient is  $2.2 \times 10^{-6}$  m/s in the case of 30:70 (column with bed depth 18 cm), CTBM:CBM loaded column, while the mass transfer coefficient decreases to  $1.9 \times 10^{-6}$  m/s when the CTBM:CBM loaded column is 70:30, having a bed depth of 27 cm.

Real-life groundwater sample was subjected for a dynamic column run, at a flow rate of 60 mL/min, with a column of 50:50 loaded adsorbent of CTBM and CBM (Fig. 5(d)). The fluoride concentration in the feed was measured as 3.6 mg/L. The breakthrough and exhaustion time were 20 h (number of bed volumes, 510) and 25 h (number of bed volumes, 637), respectively. The predicted breakthrough and exhaustion times were 16 h (number of bed volumes, 408) and 28 h (number of bed volumes, 713). Values of other parameters, such as pH, conductivity, total dissolved solids (TDS), different ions, and microbes, are presented in Table 3. The dynamic column run was able to remove fluoride and pathogen simultaneously from the feed until breakthrough is attained. For example, the microbial contamination in the feed was  $5.8 \times 10^4$  CFU/mL, which was absent in filtrate. pH of the drinking water remained within the regulatory limits (6.5–7.5, according to Indian standards). Reduction in electrical conductivity, total dissolved solids, chlorine, bromine, and nitrate was observed. However, there was an increase in aluminum, calcium, and phosphate in the drinking water, though it remained well within limits. In order to investigate leaching of various compounds from the adsorbent to the filtrate stream during dynamic run, concentration of various elements, like aluminum, calcium, sulfate, and phosphate, was measured in the filtrate for a specific experimental condition (50:50 CTBM- and CBM-loaded column, 30 mL/min and 5 mg/L artificially spiked fluoride feed). It was observed that the concentration of aluminum, calcium, and phosphate remained well within safety limits (see Fig. 5(e)). However, leaching of sulfate was observed for the first 6 h, i.e., 17% of breakthrough time (34 h). For the rest of the period, the concentration lies well within the safe limits.

Among different mathematical entities calculated for characterizing column run, there is a factor known as number of bed volume (NBV) which can highly be used to scale up a process. The factor, which is the ratio of volume of water

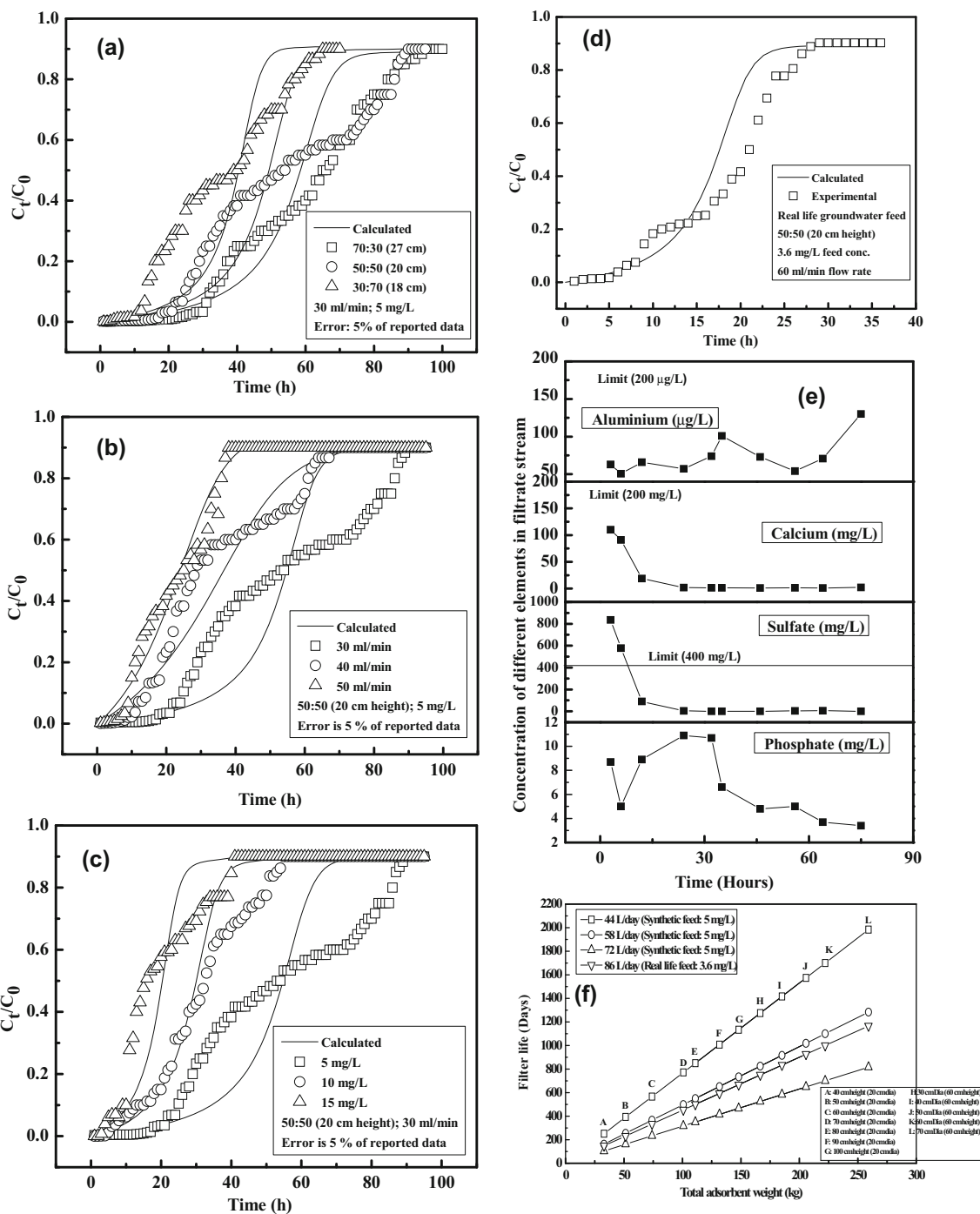


**Fig. 5** (a) Effect of bed height, (b) flow rate, (c) inlet concentration on the uptake of fluoride by chemically treated CBM, and (d) behavior of column in presence of real-life feed. (e) Leaching of various ions from

50:50 (CBM:CTBM) loaded column with 30 mL/min and 5 mg/L concentration. (f) Scale-up study of real-life feed

treated until breakthrough to the bed volume, can be evaluated for a column condition and the bed volume can be altered to find out breakthrough volumes at higher adsorbent loading. This method is employed to calculate the amount of adsorbent and the filter life for a different flow rate and influent concentration. Corresponding findings are reported in Fig. 5(f). It can be observed that the variation in column diameter and height

leads to variation in filter life at different flow rates. For example, in the case of designed filter having 100-cm height and 20-cm diameter (L/D ratio of 5), 150 kg of net adsorbent weight, i.e., 75 kg of CTBM and 75 kg of CBM, is required to have a filter life of 1124 days (3 years) at 44 L/day of drinking water with fluoride concentration of 5 mg/L during continuous operation (point G in Fig. 5(f)). However, the filter

**Table 3** Filtrate concentration after column run for real-life feed

Parameter	Feed	Filtrate (after 1 h)	Filtrate (at breakthrough, i.e., 20 h)	Allowable limits
pH	8.4	7.8	7.9	6.5–8.5
Total dissolved solids (mg/L)	283	250	234	500
Cl <sup>-</sup> (mg/L)	34.8	25.1	23.1	250
Br <sup>-</sup> (mg/L)	0.6	0.5	0.4	–
NO <sub>2</sub> <sup>-</sup> (mg/L)	3.8	0.3	0.1	45
PO <sub>4</sub> <sup>2-</sup> (mg/L)	0.3	0.2	2	–
SO <sub>4</sub> <sup>2-</sup> (mg/L)	5.6	1323	9.3	400
Ca <sup>2+</sup> (mg/L)	16	170	18	200
Al <sup>3+</sup> (μg/L)	20	85	25	100
F <sup>-</sup> (mg/L)	3.1	0.0048	1.5	1.5
Microorganism (CFU/mL)	5.8 × 10 <sup>4</sup>	0	0	0

life decreases to 733 days (2 years) and 668 days (1.8 years), when the flow rate is increased to 58 and 72 L/day, respectively. For a real-life feed (concentration of 3.6 mg/L), the expected filter life is 465 days (1.3 years) with the flow rate being maintained at 86 L/day.

**Comparison with other adsorbents**

Adsorption capacities of different aluminum- and calcium-coated charcoals and natural products are shown in Table 4. Two novel features of CTBM compared to other adsorbents are clearly observed from this table. First, simultaneous chemical treatment of charcoal precursor with calcium and aluminum has been attempted for the first time in this work. Second, the fluoride adsorption capacity is the highest in the case of CTBM. Aluminum-coated bone charcoal has been used for fixed-bed study and the uptake capacity in dynamic mode is

3.3 mg/g (Rojas-Mayorga et al. 2015). However, in the case of a 50:50 (CTBM:CBM) packed column, the dynamic uptake capacity is 4.8 mg/g (see Table S5, in the Supplementary Section), which is comparatively higher. It is obvious that during treatment of charcoal precursor with only aluminum compounds, the treatment solution turns acidic, initiating calcium leaching from the charcoal, thereby lowering the effective fluoride uptake capacity. This is observed in the case of aluminum with iron-treated wood charcoal (13.6 mg/g) (Tchomgui-Kamga et al. 2010a, b) and aluminum-treated activated bamboo charcoal (21 mg/g) (Wendimu et al. 2017). Similar observations are also reported in the case of activation of cow bone char by hydrochloric acid and subsequent treatment with aluminum chloride. Fluoride uptake capacity is reported to be 6.2 mg/g during acid activation that remains invariant after treatment with aluminum, due to leaching of calcium from apatite content (Nigri et al. 2017). Also, the

**Table 4** Comparison of uptake capacity of CBM and CTBM with other adsorbents

Adsorbent	Adsorption capacity (mg/g)	Reference
Peroxide-treated bone meal	2.2	Gao et al. 2009
Aluminum- and iron-treated corrosion products	0.48	García-Sánchez et al. 2013
Aluminum-doped cow bone char	6.4	Nigri et al. 2017
Acid-washed cow bone char	6.2	Nigri et al. 2017
Aluminum-doped bone charcoal	3.3 (dynamic mode)	Rojas-Mayorga et al. 2015
Calcium-treated wood charcoal	19.6	Tchomgui-Kamga et al. 2010a, b
Aluminum-treated wood charcoal	13.6	Tchomgui-Kamga et al. 2010a, b
Aluminum-treated activated bamboo charcoal	21	Wendimu et al. 2017
CBM	14	This study
CTBM	150	This study

corrosion products are rich in passive iron. Further treatment with aluminum and iron does not help in increasing its fluoride uptake capacity (0.48 mg/g) (García-Sánchez et al. 2013). Moreover, there is high probability of iron leaching to the treated stream during dynamic treatment. When wood charcoal is treated with calcium only, the material has an uptake capacity of 19.6 mg/g (Tchomgui-Kamga et al. 2010a, b). Calcium coated on the charcoal surface is not active in the uptake of fluoride. Peroxide treatment of raw bone meal may result in leaching of maximum calcium content, thereby lowering its effective fluoride uptake capacity (2.2 mg/g) (Gao et al. 2009). Apart from this, all these materials have issue regarding scalability, complexity in manufacturing, clogging of filter beds, and most importantly cost. This makes the synthesized adsorbent, i.e., CBM (12 mg/g) and CTBM (150 mg/g), unique and highly beneficial in fluoride treatment and microbial decontamination of groundwater.

### Industrial application and economic analysis of the adsorbent

The adsorbent has calcium and aluminum in its composition as observed from the elemental analysis. Apart from fluoride removal, it can be used for varieties of other hazardous contaminant removal, such as heavy metals (Piccirillo et al. 2017) and oily and solid suspensions for processing industrial discharges (Amiri et al. 2013). Once the adsorbent's activity is completed, it can be used for other applications such as production of carbon disulfide gas, sodium cyanide, and carbides (Emrich 2013). The used adsorbent can also be used as fuel in cement industry, in household, and also for smelting and sintering iron ores (Bhatnagar 2012).

The yield of the carbonized product is 61% (refer to Table S1a), which is comparatively higher than most of the adsorbent. For example, the yield of activated carbon from pine cone is 52% (Khalili et al. 2015); tamarind seed, 40% (Gupta and Babu 2009); and olive stones, 36% (Yakout and El-Deen 2016). Cost of conventional defluorinating agents, like activated alumina is Rs. 205/kg (size, 0.5–2 mm; source: Global Adsorbents, Kolkata, India) and Rs. 400/kg (size, 0.5–2 mm; source: Akshar Chem Activated Alumina, Kolkata, India). Cost of activated charcoal is Rs. 250/kg (source: Unitech Water Technologies, Kolkata, India) and Rs. 210/kg (source: Acuro Organics Limited, Kolkata, India). However, the present defluorinating material/medium, i.e., CTBM, is economic having a net cost of 133 INR/kg (equivalent to 2 USD/kg) (refer to Table S7).

### Conclusions

Preparation, characterization, and defluorination application of chemically treated carbonized bone meal were presented

in this work. Partially carbonized bone meal was chemically treated by aluminum sulfate and calcium oxide solution to enhance the fluoride adsorption capacity. Optimum operating conditions for carbonization as well as chemical treatment were established. Maximum adsorption capacity of CTBM was found to be 150 mg/g and the adsorbent had significant antibacterial property. Hydroxylapatite and aluminum phases in CTBM were responsible for enhanced uptake fluoride. Maximum fluoride removal capacity was observed at pH 6.1, 0.15-mm particle size, and 5-g/L dosage. Among competing ions, presence of phosphate interfered fluoride uptake significantly. Uptake capacity was reduced by 31% after three regeneration cycles. Uptake of fluoride by CTBM was exothermic and chemisorption in nature. Adsorption kinetics was adequately explained by shrinking core model. Continuous fixed-bed experiments showed that the breakthrough time was 20 h (number of bed volumes, 510) for 72-L/day flow rate, 3.6-mg/L feed fluoride concentration, and 100-g (50-g CBM and 50-g CTBM) adsorbent loading during treatment of real-life contaminated groundwater. A convection-diffusion-pore adsorption model was used to simulate the fixed-bed column data, and an appropriate scale-up study was performed. This study revealed that 150 kg of adsorbent is required to fabricate a filter having an expected life of 465 days at 86 L/day. An economic analysis indicated that the material is cost-effective compared to most of the defluorinating agents in the market.

**Acknowledgements** The authors would also like to acknowledge the help of Amarnath Dutta and Kallol Paul for their help in carrying some of the experimental works.

**Funding information** This work is supported by a grant from the Department of Science and Technology, New Delhi, Government of India, under the scheme no: DST/TM/WTI/2K15/22(G) dated 31-03-2016. Any opinions, findings, and conclusions expressed in this paper are those of the authors and do not necessarily reflect the views of DST.

**Nomenclature** *A*, amount of bone meal before carbonization (g); *B*, amount of bone meal after carbonization (g); *C<sub>0</sub>*, initial fluoride concentration (mg/L); *C<sub>e</sub>*, equilibrium fluoride concentration (mg/L); *C<sub>ads</sub>*, adsorbed fluoride concentration (mg/L); *C<sub>des</sub>*, desorbed fluoride concentration (mg/L); *D*, desorption percentage (%); *m*, mass of adsorbent used (g); *q<sub>e</sub>*, equilibrium uptake capacity (mg/g); *v*, volume of adsorbate solution used (L); *yield*, yield percentage of carbonized bone meal (%)

### References

- Amiri MJ, Abedi-Koupai J, Eslamian S, Mousavi SF, Arshadi M (2013) Modelling Pb (II) adsorption based on synthetic and industrial wastewaters by ostrich bone char using artificial neural network and multivariate non-linear regression. *Int J Hydrol Sci Technol* 3: 221–240
- Bhatnagar A (ed) (2012) Application of adsorbents for water pollution control. Bentham Science Publishers, Bussum



- Brindha K, Elango L (2011) Fluoride in groundwater: causes, implications and mitigation measures. In: Monroy SD (ed) Fluoride properties, applications and environmental management, illustrated edn. Nova Science Publishers, New York, pp 111–136
- Chatterjee S, De S (2016) Application of novel, low-cost, laterite-based adsorbent for removal of lead from water: equilibrium, kinetic and thermodynamic studies. *J Environ Sci Health A* 51:193–203
- Chatterjee S, Sivareddy I, De S (2017) Adsorptive removal of potentially toxic metals (cadmium, copper, nickel and zinc) by chemically treated laterite: single and multicomponent batch and column study. *J Environ Chem Eng* 5:3273–3289
- Czernik S (2008) Fundamentals of charcoal production. In: IBI Conference on Biochar, Sustainability and Security
- Delgado-Velasco L, Hernández-Montoya V, Cervantes FJ, Montes-Morán MA, Lira-Berlanga D (2017) Bone char with antibacterial properties for fluoride removal: preparation, characterization and water treatment. *J Environ Manag* 201:277–285
- Deng H, Yu X (2012) Adsorption of fluoride, arsenate and phosphate in aqueous solution by cerium impregnated fibrous protein. *Chem Eng J* 184:205–212
- Dikinya O, Hinz C, Aylmore G (2008) Decrease in hydraulic conductivity and particle release associated with self-filtration in saturated soil columns. *Geoderma* 146:192–200
- Du X, Wang Y, Su X, Li J (2009) Influences of pH value on the microstructure and phase transformation of aluminum hydroxide. *Powder Technol* 192:40–46
- Emrich W (2013) Handbook of charcoal making: the traditional and industrial methods. Springer Science & Business Media, Berlin
- Faust SD, Aly OM (2013) Adsorption processes for water treatment. Elsevier, Amsterdam
- Foo KY, Hameed BH (2010) Insights into the modeling of adsorption isotherm systems. *Chem Eng J* 156:2–10
- Ganvir V, Das K (2011) Removal of fluoride from drinking water using aluminum hydroxide coated rice husk ash. *J Hazard Mater* 185:1287–1294
- Gao S, Cui J, Wei Z (2009) Study on the fluoride adsorption of various apatite materials in aqueous solution. *J Fluor Chem* 130:1035–1041
- García-Sánchez JJ, Martínez-Miranda V, Solache-Ríos M (2013) Aluminum and calcium effects on the adsorption of fluoride ions by corrosion products. *J Fluor Chem* 145:136–140
- Ghorai S, Pant KK (2005) Equilibrium, kinetics and breakthrough studies for adsorption of fluoride on activated alumina. *Sep Purif Technol* 42:265–271
- Gong WX, Qu JH, Liu RP, Lan HC (2012) Effect of aluminum fluoride complexation on fluoride removal by coagulation. *Colloids Surf A Physicochem Eng Asp* 395:88–93
- Granados ML, Poves MZ, Alonso DM, Mariscal R, Galisteo FC, Moreno-Tost R, Santamaría J, Fierro JL (2007) Biodiesel from sunflower oil by using activated calcium oxide. *Appl Catal B Environ* 73:317–326
- Guo Q, Tian J (2013) Removal of fluoride and arsenate from aqueous solution by hydrocalumite via precipitation and anion exchange. *Chem Eng J* 231:121–131
- Gupta S, Babu BV (2009) Utilization of waste product (tamarind seeds) for the removal of Cr (VI) from aqueous solutions: equilibrium, kinetics, and regeneration studies. *J Environ Manag* 90:3013–3022
- Jena PR, De S, Basu JK (2003) A generalized shrinking core model applied to batch adsorption. *Chem Eng J* 95:143–154
- Katole SB, Kumar P, Patil RD (2013) Environmental pollutants and livestock health: a review. *Vet Res Int* 1:1–3
- Khalili S, Khoshandam B, Jahanshahi M (2015) Optimization of production conditions for synthesis of chemically activated carbon produced from pine cone using response surface methodology for  $CO_2$  adsorption. *RSC Adv* 5:94115–94129
- Kim SM, Lee YJ, Bae JW, Potdar HS, Jun KW (2008) Synthesis and characterization of a highly active alumina catalyst for methanol dehydration to dimethyl ether. *Appl Catal A Gen* 348:113–120
- Kuang D, Fang Y, Liu H, Frommen C, Fenske D (2003) Fabrication of boehmite  $AlOOH$  and  $\gamma-Al_2O_3$  nanotubes via a soft solution route. *J Mater Chem* 13:660–662
- Liu Q, Guo H, Shan Y (2010) Adsorption of fluoride on synthetic siderite from aqueous solution. *J Fluor Chem* 131:635–641
- Mohapatra M, Anand S, Mishra BK, Giles DE, Singh P (2009) Review of fluoride removal from drinking water. *J Environ Manag* 91:67–77
- Moore JW (2012) Inorganic contaminants of surface water: research and monitoring priorities. Springer Science & Business Media, Berlin
- Mukherjee M, De S (2015) Reduction of microbial contamination from drinking water using an iron oxide nanoparticle-impregnated ultrafiltration mixed matrix membrane: preparation, characterization and antimicrobial properties. *Environ Sci: Water Res Technol* 1:204–217
- Mukherjee M, De S (2017) Investigation of antifouling and disinfection potential of chitosan coated iron oxide-PAN hollow fiber membrane using Gram-positive and Gram-negative bacteria. *Mater Sci Eng C* 75:133–148
- Ndiaye PI, Moulin P, Dominguez L, Millet JC, Charbit F (2005) Removal of fluoride from electronic industrial effluent by RO membrane separation. *Desalination* 173:25–32
- Nie Y, Hu C, Kong C (2012) Enhanced fluoride adsorption using Al (III) modified calcium hydroxyapatite. *J Hazard Mater* 233–234:194–199
- Nigri EM, Cechinel MA, Mayer DA, Mazur LP, Loureiro JM, Rocha SD, Vilar VJ (2017) Cow bones char as a green sorbent for fluorides removals from aqueous solutions: batch and fixed-bed studies. *Environ Sci Pollut Res* 24:2364–2380
- Nigussie W, Zewge F, Chandravanshi BS (2007) Removal of excess fluoride from water using waste residue from alum manufacturing process. *J Hazard Mater* 147:954–963
- Njoku VO (2014) Biosorption potential of cocoa pod husk for the removal of Zn (II) from aqueous phase. *J Environ Chem Eng* 2(2):881–887
- Ozsvath DL (2009) Fluoride and environmental health: a review. *Rev Environ Sci Biotechnol* 8:59–79
- Piccirillo C, Moreira IS, Novais RM, Fernandes AJS, Pullar RC, Castro PML (2017) Biphasic apatite-carbon materials derived from pyrolysed fish bones for effective adsorption of persistent pollutants and heavy metals. *J Environ Chem Eng* 5:4884–4894
- Rojas-Mayorga CK, Bonilla-Petriciolet A, Aguayo-Villarreal IA, Hernandez-Montoya V, Moreno-Virgen MR, Tovar-Gómez R, Montes-Morán MA (2013) Optimization of pyrolysis conditions and adsorption properties of bone char for fluoride removal from water. *J Anal Appl Pyrolysis* 104:10–18
- Rojas-Mayorga CK, Bonilla-Petriciolet A, Sánchez-Ruiz FJ, Moreno-Pérez J, Reynel-Ávila HE, Aguayo-Villarreal IA, Mendoza-Castillo DI (2015) Breakthrough curve modeling of liquid-phase adsorption of fluoride ions on aluminum-doped bone char using micro-columns: effectiveness of data fitting approaches. *J Mol Liq* 208:114–121
- Sellaoui L, Fraco DSP, Dotto GL, Lima EC, Lamine AB (2016) Single and binary adsorption of cobalt and methylene blue on modified chitin: application of the Hill and exclusive extended Hill models. *J Mol Liq* 233:543–550
- Sellaoui L, Dotto GL, Lamine AB, Erto A (2017a) Interpretation of single and competitive adsorption of cadmium and zinc on activated carbon using monolayer and exclusive extended monolayer models. *Environ Sci Pollut Res* 24:19902–19908
- Sellaoui L, Soetaredjo FE, Ismadij S, Lima EC, Dotto GL, Lamine AB, Erto A (2017b) New insights into single-compound and binary adsorption of copper and lead ions on treated sea mango shell: experimental and theoretical studies. *Phys Chem Chem Phys* 19:25927–25937

- Siesler HW, Ozaki Y, Kawata S, Heise HM (2008) Near-infrared spectroscopy: principles, instruments, applications. Wiley, New York
- Singha S, Sarkar U, Mondal S, Saha S (2012) Transient behavior of a packed column of *Eichhornia crassipes* stem for the removal of hexavalent chromium. *Desalination* 297:48–58
- Sivasankar V, Rajkumar S, Muruges S, Darchen A (2012) Tamarind (*Tamarindus indica*) fruit shell carbon: a calcium-rich promising adsorbent for fluoride removal from groundwater. *J Hazard Mater* 225:164–172
- Sujana MG, Pradhan HK, Anand S (2009) Studies on sorption of some geomaterials for fluoride removal from aqueous solutions. *J Hazard Mater* 161:120–125
- Sulaymon AH, Abid BA, Al-Najar JA (2009) Removal of lead copper chromium and cobalt ions onto granular activated carbon in batch and fixed-bed adsorbers. *Chem Eng J* 155:647–653
- Tang Y, Guan X, Wang J, Gao N, McPhail MR, Chusuei CC (2009) Fluoride adsorption onto granular ferric hydroxide: effects of ionic strength, pH, surface loading, and major co-existing anions. *J Hazard Mater* 171(1):774–779
- Tchomgui-Kamga E, Ngameni E, Darchen A (2010a) Evaluation of removal efficiency of fluoride from aqueous solution using new charcoals that contain calcium compounds. *J Colloid Interface Sci* 346:494–499
- Tchomgui-Kamga E, Alonzo V, Nansou-Njiki CP, Audebrand N, Ngameni E, Darchen A (2010b) Preparation and characterization of charcoals that contain dispersed aluminum oxide as adsorbents for removal of fluoride from drinking water. *Carbon* 48:333–343
- Tor A, Danaoglu N, Arslan G, Cengeloglu Y (2009) Removal of fluoride from water by using granular red mud: batch and column studies. *J Hazard Mater* 164:271–278
- Turner BD, Binning PJ, Sloan SW (2010) Impact of phosphate on fluoride removal by calcite. *Environ Eng Sci* 27:643–650
- Wang SG, Ma Y, Shi YJ, Gong WX (2009) Defluoridation performance and mechanism of nano-scale aluminum oxide hydroxide in aqueous solution. *J Chem Technol Biotechnol* 84:1043–1050
- Wendimu G, Zewge F, Mulugeta E (2017) Aluminium-iron-amended activated bamboo charcoal (AIAABC) for fluoride removal from aqueous solutions. *J Water Process Eng* 16:123–131
- World Health Organization (2004) Guidelines for drinking-water quality. World Health Organization, Geneva
- Wu ZL, Yang H, Jiao FP, Liu Q, Chen XQ, Yu JG (2015) Carbon nanoparticles pillared multi-walled carbon nanotubes for adsorption of 1-naphthol: thermodynamics, kinetics and isotherms. *Colloids Surf A Physicochem Eng Asp* 470:149–160
- Yakout SM, El-Deen GS (2016) Characterization of activated carbon prepared by phosphoric acid activation of olive stones. *Arab J Chem* 9:S1155–S1162
- Yu X, Tong S, Ge M, Zuo J (2013) Removal of fluoride from drinking water by cellulose@ hydroxyapatite nanocomposites. *Carbohydr Polym* 92:269–275
- Zhang Y, Venugopal JR, El-Turki A, Ramakrishna S, Su B, Lim CT (2008) Electrospun biomimetic nanocomposite nanofibers of hydroxyapatite/chitosan for bone tissue engineering. *Biomaterials* 29:4314–4322